AIAA SciTech Forum
23-27 January 2023, National Harbor, MD & Online
AIAA SCITECH 2023 Forum

10.2514/6.2023-2609

Numerical Study of Co-Flow-Jet Distribution along the Span of Finite Wing

Zhijin Lei, *Gecheng Zha †
Dept. of Mechanical and Aerospace Engineering
University of Miami, Coral Gables, Florida 33124

Abstract

This paper numerically studies the spanwise distribution of Co-Flow Jet (CFJ) for a straight wing at freestream Mach number of 0.30, C_μ=0.03 and 0.06 at angles of attack (AOA) of 5° and 14°. Five configurations with different CFJ distributions along the wing span with an aspect ratio (AR) of 10 are investigated. Among these configurations, CFJ-covered suction surface area varies from 38.5% to 90% of the wing span in continuous or discrete distribution along the span. The numerical simulations employ the validated in-house CFD code FASIP, which utilizes a 3D RANS solver with Spalart-Allmaras (S-A) turbulence model, 3rd order WENO scheme for the inviscid fluxes, and 2nd order central differencing for the viscous terms.

The study shows that, due to the existence of vortex near the tip, CFJ in this region does not provide as large lift enhancement as in near-root places in the span, and an area including as large as 20% of wing span can thus be freed from CFJ device to satisfy requirements from weight or structural considerations. Also with the help of tip vortices, under normal working condition at a small angle of attack of 5°, with 61.5% of suction surface area free from coflow jet, the CFJ lift enhancement effect can decrease for a slighter 49.8%.

Meanwhile, with constant C_μ, the performance of wings mounted with discrete CFJ is penalized with the increasing size of gaps between the discrete jets. Narrow gaps between injection and suction slots of parallel CFJ sets only lead to minor penalty at small AoAs. Still, to optimize the lift performance at large AoAs, these gaps are expected to be minimized or eliminated. There is an exception that at stall condition with not enough C_μ to eliminate the separation, which is abnormal, a "concentrated" C_μ distribution method can maintain some lift enhancement, but generally speaking, when the CFJ is discretized, the larger angle of attack has more performance penalty.

Nomenclature

CFJ	Co-flow Jet
AoA	Angle of Attack
AR	Aspect Ratio
C_μ	Jet Momentum Coefficient $\dot{m}_j\, U_j/(q_\infty\, S_{ref})$
c	Chord Length
l_{duct}	Slot Width
M	Mach Number
P	Static Pressure
$\overline{P}$	Mass-averaged Static Pressure
P_c	Power Coefficient

* Ph.D. Candidate
† Professor, ASME Fellow, AIAA associate Fellow

P_t	Total Pressure
P_tR	Total Pressure Ratio
$\overline{P_t}$	Mass-averaged Total Pressure
q	Dynamic Pressure, $= 0.5\,\rho\,U^2$
R	CFJ-Coverage Parameter
S	Planform Area
s	Half Wingpan
T_t	Total Temperature
V	Flow Velocity
γ	Specific Heat Ratio
η	Pump Efficiency
ρ	Air Density
∞	Free Stream Conditions
$_j$	Jet Value
$_{max}$	Maximum Value
$_{min}$	Minimum Value
$_{mass-av}$	Mass Average Value
$_{inj}$	Value at Injection slot
$_{suc}$	Value at Suction slot
LE	Leading Edge
SST	Suction Surface Translation
TE	Trailing Edge

1 Introduction

The CFJ active flow control airfoil [1, 2, 3, 4, 5, 6, 7, 8, 9, 10, 11, 12] achieves large lift augmentation, stall margin increase, drag reduction at low energy expenditure. In a CFJ airfoil, an injection slot near the leading edge (LE) and a suction slot near the trailing edge (TE) on the airfoil suction surface are created. As shown in Fig. 1, a small amount of mass flow is drawn into the suction duct, pressurized and energized by micro compressor actuators, and then injected near the LE tangentially to the main flow via an injection slot. The whole process does not add any mass flow to the system and hence is a zero-net-mass-flux(ZNMF) flow control.

For a straight wing, the design principle of elliptic lift distribution along the span would minimize the tip load to reduce induced drag. This leads to a question in the CFJ wing design: How much does the wing span actually need to be covered by CFJ? In another word, is it more efficient to avoid CFJ in the wing tip region?

In the current CFD simulation of a straight wing with large aspect ratio(AR), a continuous open slot along the span is often used to facilitate the mesh generation and save CPU time. However in reality, the CFJ will be distributed along the span with individual sets, where each set will have a micro-compressor and its associated suction / injection duct, as shown in Fig. 1(b). If CFJ sets are placed next to each other ideally with no gap, it would perform as a continuous slot along the span, just like what has been simulated sufficiently. However, when the CFJ sets are placed with large gaps between them in order to reduce micro compressor actuators, will there be and what is the gap size effect on the 3D wing performance, especially as angles of attack(AoA) changes?

The purpose of this paper is to investigate the CFJ spanwise distribution effect for a finite wing to answer the questions above. The focus is more on the cruise condition with low AoA and C_μ. This knowledge would be very

useful for 3D wing design.

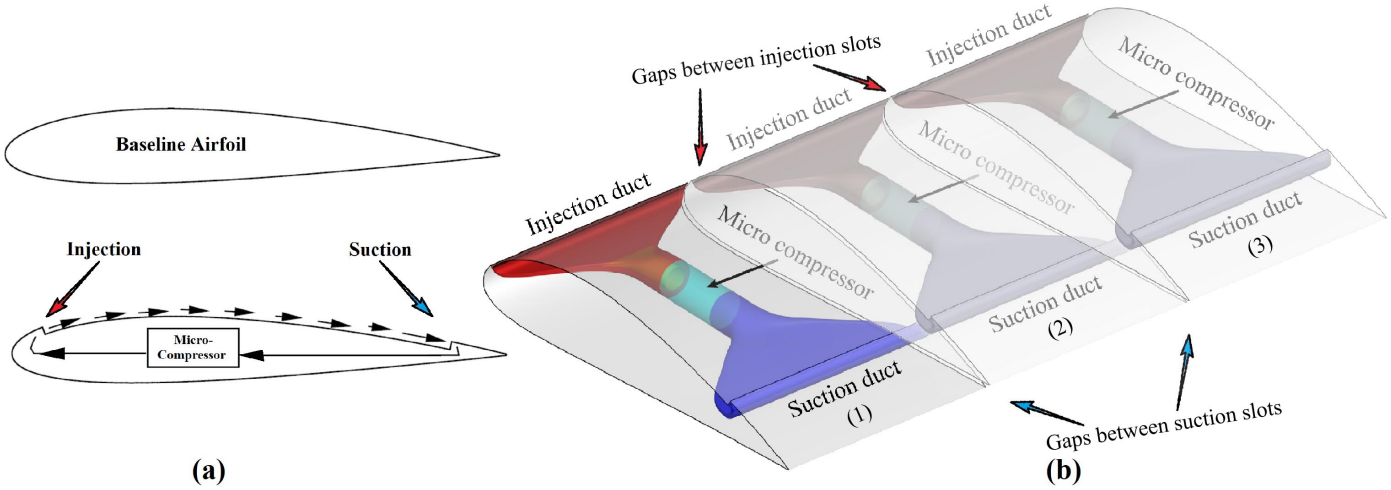

Figure 1: Schematic plot of a conceptual CFJ airfoil(a) and a wing mounted with three CFJ sets(b).

2 CoFlow Jet Concept and Parameters

The jet momentum coefficient C_μ, is used to quantify the jet intensity, which is defined as:

$$C_\mu = \frac{\dot{m} V_j}{\frac{1}{2}\rho_\infty {V_\infty}^2 S_{ref}} \tag{1}$$

where $\dot{m}$ is the injection jet mass flow rate, V_j is the mass-averaged injection velocity, ρ_∞ and V_∞ denote the free stream density and velocity, and S_{ref} is the planform area of the airfoil. For discrete CFJs used along the span, the numerator is the summation of all the jet momentums.

The power consumption is determined by the jet mass flow and total enthalpy change as the following:

$$P = \dot{m}(H_{t1} - H_{t2}) \tag{2}$$

where H_{t1} and H_{t2} are the mass-averaged total enthalpy in the injection cavity and suction cavity respectively, P is the power required by the micro-compressor actuators and $\dot{m}$ the jet mass flow rate.

The total power can be expressed with the pump efficiency η and total pressure ratio of the pump $\Gamma = \frac{P_{t1}}{P_{t2}}$ as:

$$P = \frac{\dot{m} C_p T_{t2}}{\eta}(\Gamma^{\frac{\gamma-1}{\gamma}} - 1) \tag{3}$$

where γ is the specific heat ratio equal to 1.4 for air, the power coefficient is expressed as:

$$P_c = \frac{P}{\frac{1}{2}\rho_\infty V_\infty^3 S_{ref}} \tag{4}$$

The lift-drag ratio $\frac{C_L}{C_D}$ of a CFJ-wing still reflects the aerodynamic performance, but no longer reflects the energy relation of system since CFJ active flow control provides extra energy other than engine. For a CFJ-activated wing, a corrected aerodynamic efficiency $(\frac{C_L}{C_D})_c$ is defined to denote the energy expenditure meaning of typical lift-drag ratio:

$$(\frac{C_L}{C_D})_c = \frac{C_L}{C_D + P_c.} \tag{5}$$

3 Numerical Algorithms and Meshes

The in-house high order CFD code Flow-Acoustics-Structure Interaction Package (FASIP) is used to solve the 3D Reynolds averaged Navier-Stokes (RANS) equations. A 3rd order WENO scheme for the inviscid flux [13, 14, 15, 16, 17] and 2nd order central differencing for the viscous terms [14, 16] are employed to discretize the Navier-Stokes equations. The low diffusion E-CUSP scheme used as the approximate Riemann solver suggested by Zha *et al* [18] based on the flux vector splitting scheme of Zha and Bilgen[19] is utilized with the WENO scheme to evaluate the inviscid fluxes. Implicit time marching using Gauss-Seidel line relaxation is used to achieve a fast convergence rate [20]. Parallel computing with domain partitioning is implemented to save wall clock simulation time [21]. The FASIP code is intensively validated for CFJ simulations and many steady and unsteady flows [3, 4, 6, 12, 22, 23, 24, 25, 21, 26, 27].

To achieve zero-net mass-flux with the CFJ flow control, the suction mass flow must be equal to the injection mass flow. The injection total pressure is iterated to match the C_μ specified and the suction static pressure is iterated to match the mass flow rate [8].

The farfield are meshed using "O-" topology. For all geometries, the mesh size is 200×320×80 in the spanwise, around the airfoil, and radial directions respectively. The total mesh size of each geometry is 6.56 millions points, and is split into 432 blocks for the parallel computation. Most of the first grid point on the duct surface is placed at $y+ \approx 1$. A sketch of mesh and surface mesh details near wall boundary are shown in Fig. 2.

Table 1: Mesh Characteristics

Parameter	Value
Mesh Size	6.56×10^6 Cells
Farfield Radius	$63c$
Farfield in Spanwise Direction	$35c$
Nodes around Airfoil	320
Nodes Distributed along Spanwise Direction on the Wing	200
Boundary Layer Spacing	$8 \times 10^{-6}c$

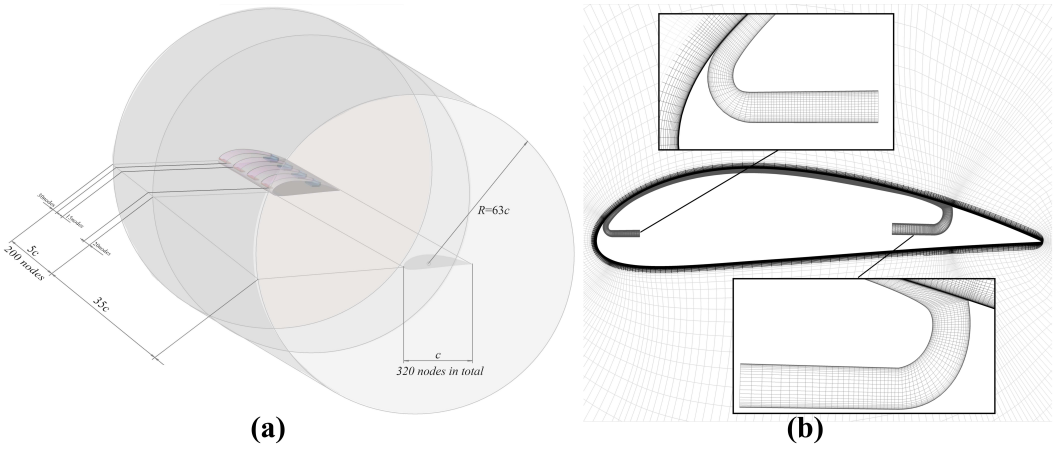

Figure 2: Schematic of mesh topology, 4-CFJ as an example(a); surface mesh around the wing and CFJ duct(b).

A mesh dependence analysis is done on each geometry and proves that the mesh size used as above is all accurate and acceptable.

4 Results and Discussion

4.1 Baseline Geometry and Flow Condition Setup

A straight wing with constant chord, zero sweep, and AR of 10 based on a profile of NACA-6421 airfoil is used as baseline geometry. All studies are under freestream Mach number of 0.30. A small AoA of 5° representing cruise condition and a large AoA of 14° representing a maneuver condition are simulated. For CFJ cases, a moderate C_μ of 0.03 is adopted for small AoA conditions, while an increased C_μ of 0.06 is used to remove flow separation at the large AoA.

Table 2: Flow Condition

Parameter	Value
M_∞	0.30
Re, based on Chord	2.67×10^6
CFJ C_μ, for AoA of 5°	0.03
CFJ C_μ, for AoA of 14°	0.06

For the wing configurations that contains multiple CFJ sets, C_μ is uniformly distributed to every CFJ set.

4.2 Study of CFJ in Wing Tip Region

For a finite wing, CFJ in the tip region is expected to provide less lift and efficiency enhancement due to the tip vortex effect, especially at large AoAs. To study the tip vortex effect, three continuous open CFJ slots covering the full span, 90% span, and 80% span as shown in Fig. 3 are studied.

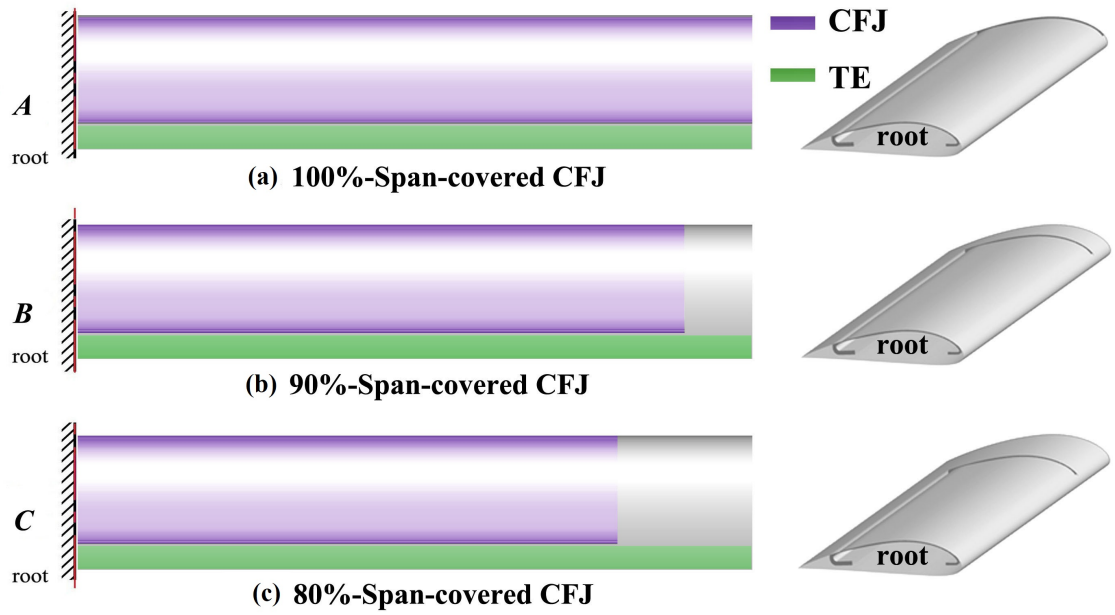

Figure 3: Three wing configurations with CFJ covered by 100% span, 90% span, and 80% span.

The CFJ injection and suction duct shapes are the same for all the configurations studied in this paper. The injection slot height is 1% of chord length, the suction slot width is 2.48% of chord length, and suction surface translation(SST) is 1% of chord length. As shown in Fig. 3 on the right, the configurations have a step created by the recessed CFJ SST between the CFJ slot and the non-CFJ geometry. The non-CFJ geometry is formed by the NACA6421 airfoil.

Table 3: Performance of Varied Solid Tip Spans of CFJ-NACA-6421 at M_∞=0.3, AoA=5°, CFJ C_μ=0.03

Open-CFJ Wing Geometry	C_L	δC_L	C_L/C_D	$(C_L/C_D)_c$	$({C_L}^2/C_D)_c$	P_c	PR	V_{inj}/V_∞
100%-Span-covered CFJ (A)	1.112	0	23.26	19.06	21.21	0.0105	1.051	1.158
90%-Span-covered CFJ (B)	1.109	-0.3%	23.51	19.15	21.25	0.0107	1.054	1.249
80%-Span-covered CFJ (C)	1.098	-1.3%	23.59	19.04	20.91	0.0111	1.060	1.295
Baseline NACA-6421	0.838	-24.6%	19.96	19.96	16.73	0.000	-	-

Table 3 compares the CFJ with full span, 90% span, and 80% with the baseline wing with no CFJ. All the CFJ wing configurations use the same $C\mu$ of 0.03. Table 3 indicates that at the cruise AoA of 5°, the overall aerodynamic performance is insensitive to the distribution of CFJ within 20% of the tip region with the C_L and $(C_L/C_D)_c$ variation within 1.3%. Similar to the findings by Wang and Zha[29], all the CFJ wings have over 31% higher Lift coefficient than the uncontrolled baseline wing. But the $(C_L/C_D)_c$ drops slightly by 4.5%. The productivity efficiency $(C_L^2/C_D)_c$ is increased more than 25%. Since the C_μ is the same for all the CFJ configurations, the 80% span of CFJ has smaller area of the injection slot, thus 11.8% higher injection velocity and 5.7% higher CFJ power coefficient. The 90% span CFJ configuration gives a slightly higher $(C_L/C_D)_c$ than the 100% span CFJ and 80% span CFJ.

Table 4 compares the three CFJ models at another typical cruise AoA of 2°, and indicates similar results; the overall aerodynamic performance is insensitive to the distribution of CFJ within 20% of the tip region, with the C_L and $(C_L/C_D)_c$ variation within only 2.0%.

Table 4: Performance of Varied Solid Tip Spans of CFJ-NACA-6421 at M_∞=0.3, AoA=2°, CFJ C_μ=0.03

Wing Geometry	C_L	δC_L	C_L/C_D	$(C_L/C_D)_c$	$(C_L{}^2/C_D)_c$	P_c	PR	V_{inj}/V_∞
CFJ-A	0.836	0	27.85	19.32	16.16	0.0132	1.063	1.263
CFJ-B	0.831	-0.6%	27.99	19.33	16.06	0.0133	1.067	1.194
CFJ-C	0.819	-2.0%	28.02	19.02	15.70	0.0135	1.073	1.138

The configuration B with 90% CFJ span is thus used as the reference configuration for the discrete CFJ distribution study in the next section. More study on the CFJ effect in the tip region with variation of AoA and C_μ is in progress and will be reported in future.

4.3 Configurations with Discrete CFJ Distributions

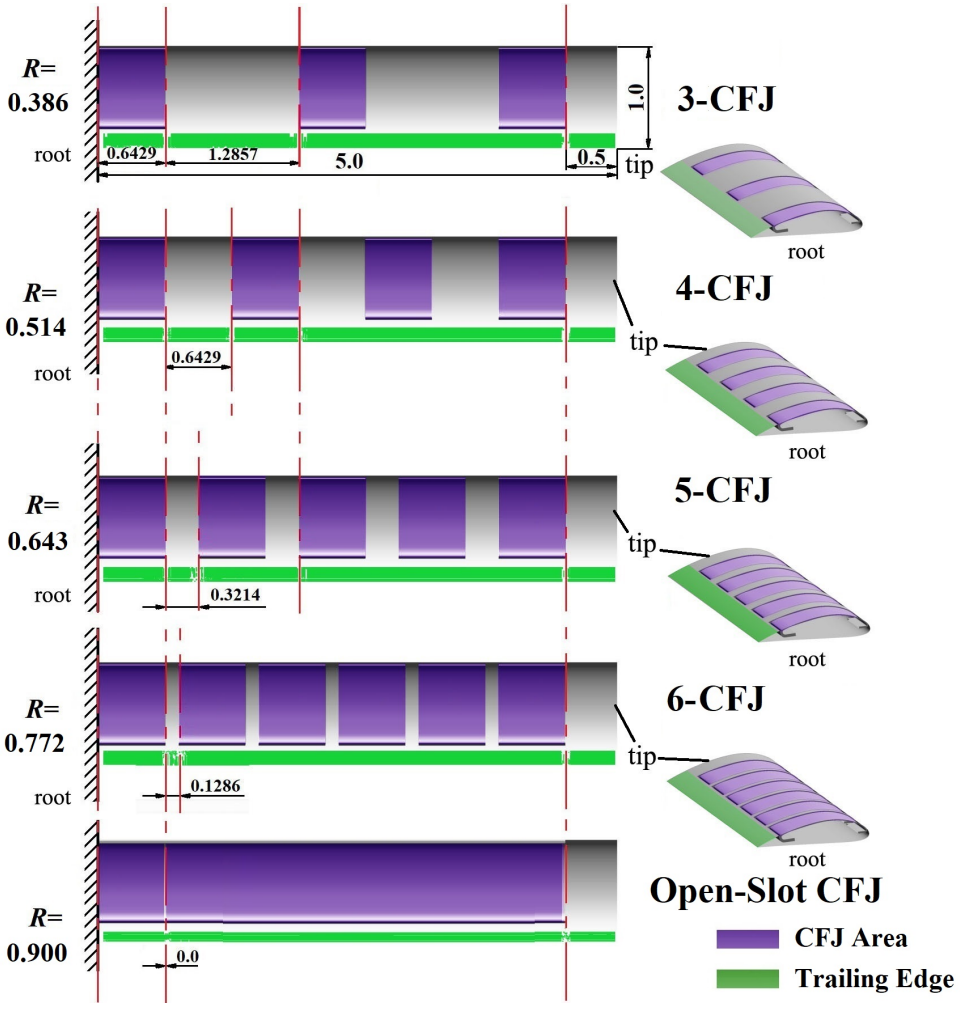

Figure 4: Dimension of Discrete CFJ geometries.

This section describes the discrete CFJ configurations. The CFJ covered area is defined by parameter R representing the percentage of the CFJ area in the whole wing planform area.

$$R = \frac{\Sigma S_{CFJ}}{\Sigma S_{ref}} \tag{6}$$

Four discrete CFJ configurations 3-CFJ, 4-CFJ, 5-CFJ and 6-CFJ are given in Fig. 6 with the detailed dimensions labeled. In this study, each individual CFJ set has a span of $S_{CFJ} = 0.6429c$. The four configurations are created with gap size equal to $2S_{CFJ}$ (3-CFJ), $1S_{CFJ}$ (4-CFJ), $0.5S_{CFJ}$ (5-CFJ), and $0.2S_{CFJ}$ (6-CFJ) respectively to conduct a trade study of the gap size effect.

4.4 Flow Characteristics of Model 6-CFJ

To study the effect of discrete CFD distribution, we begin with the 6-CFJ configuration shown in Fig. 4, which has the smallest gap of $0.2c$ between the CFJ sets. The lift, drag and power coefficient of the 6-CFJ at an ideal cruise condition, M_∞=0.3, are compared with the continuous CFJ configuration B and the baseline wing with no CFJ in Table 5.

The discrete 6-CFJ configuration has the gap of $0.2c$ and the CFJ covered area of 77.2%. It can be seen that, at C_μ=0.03 and AoA=5° compared with the continuous CFJ-B configuration, the lift coefficient is decreased by 3.7% and the $(C_L/C_D)c$ is decreased by 4.3%. The penalty is primarily from the increased CFJ power coefficient due to smaller injection area with higher injection velocity, which creates higher total pressure loss. However, when the AoA increases, performance of 6-CFJ including lift coefficient, C_L/C_D and $(C_L/C_D)c$ significantly deteriorated.

Table 5: Performance of 6-CFJ-NACA-6421 and Comparisons at M_∞=0.3.

Model	Flow Condition	C_L	δC_L	C_D	C_L/C_D	P_c	$(C_L/C_D)_c$
CFJ-B	C_μ=0.03, AoA=5°	1.109	-	0.0471	23.51	0.0107	19.154
6-CFJ	C_μ=0.03, AoA=5°	1.068	-3.70%	0.0464	23.01	0.0119	18.331
Baseline NACA-6421	AoA=5°	0.838	-24.4%	0.0420	19.952	0.000	19.952
CFJ-B	C_μ=0.06, AoA=14°	1.966	-	0.1372	14.329	0.0155	12.875
6-CFJ	C_μ=0.06, AoA=14°	1.690	-14.1%	0.1483	11.396	0.0286	9.553
Baseline NACA-6421	AoA=14°	1.403	-28.6%	0.1130	12.416	0.000	12.416

Fig. 5 compare the aerodynamic performance and flow fields of the configurations of continuous CFJ-B, discrete 6-CFJ, and the baseline wing with no CFJ. For both the CFJ configurations, a C_μ of the 0.06 is required to keep the flow unstalled. The CFJ-B wing has no flow separation at AoA of 14°, but the 6-CFJ has some minor flow separation near the root in the gap regions. The baseline configuration has a flow separation at AoA of 14° and is its stall AoA.

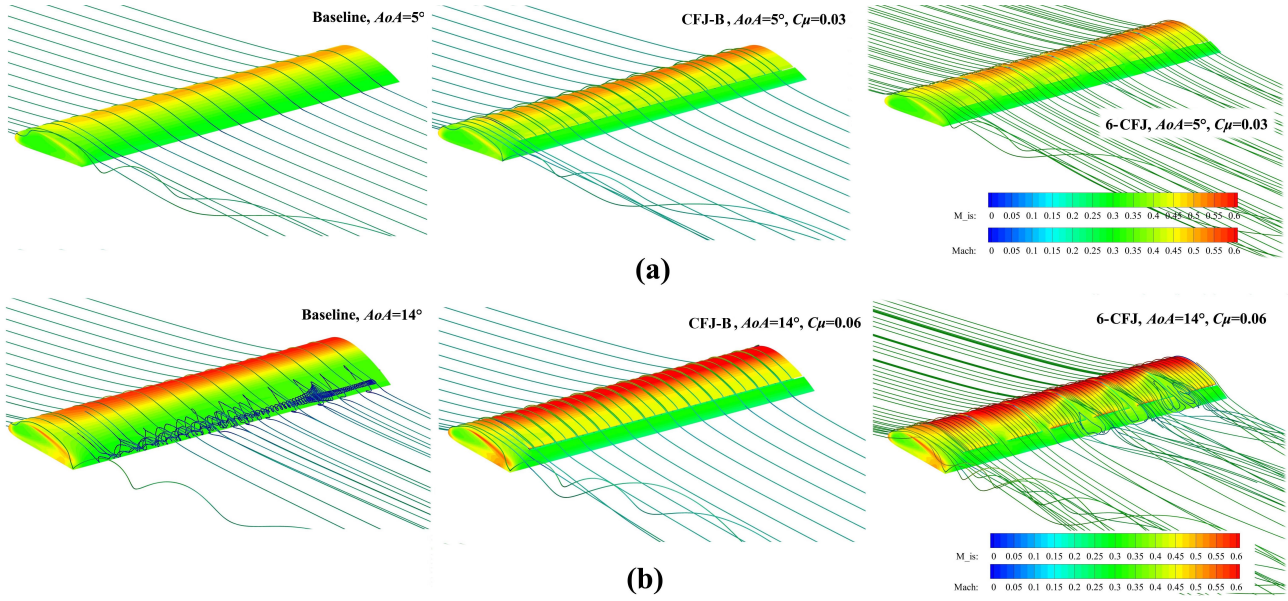

Figure 5: Streamline around the suction surface of 6-CFJ at varied flow conditions.

The wing surfaces in Fig. 5 are contoured by isentropical Mach number distribution, which reflects the pressure distribution. The M_{is} distributions on 6-CFJ are clearly re-depicted in Fig. 6 at both flow conditions. It can be seen that, at ideal cruise condition AoA=5° and C_μ=0.03, the improvement introduced by CFJ declines from root to tip while the designated C_μ on every CFJ set is identical. However, as shown in Fig. 7(a), to keep this C_μ on this tip CFJ set, the contribution to pump power on CFJ 6-6 is the largest of all. This suggests that compared with the root CFJ sets, like 6-1 or 6-2, the C_μ given to tip CFJ set 6-6 is redundant and unnecesssary. However, by reasonably allocating less C_μ to 6-6 and more to 6-1 and 6-2, the C_L and C_L/C_D is only slightly increased. The best method seems to be keep CFJ ducts near root region combined.

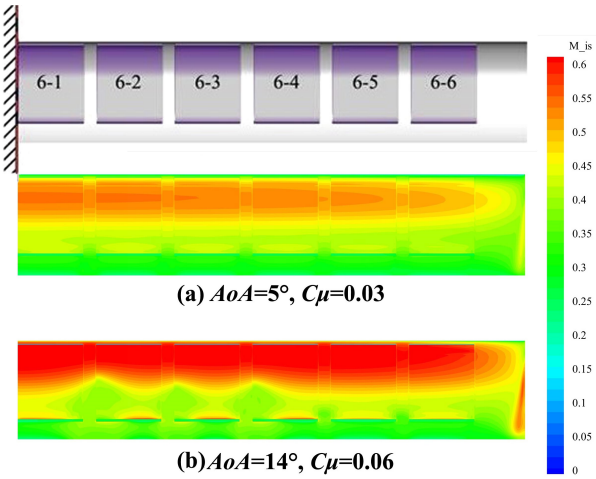

Figure 6: Isentropical Mach number distribution on the suction surface of 6-CFJ.

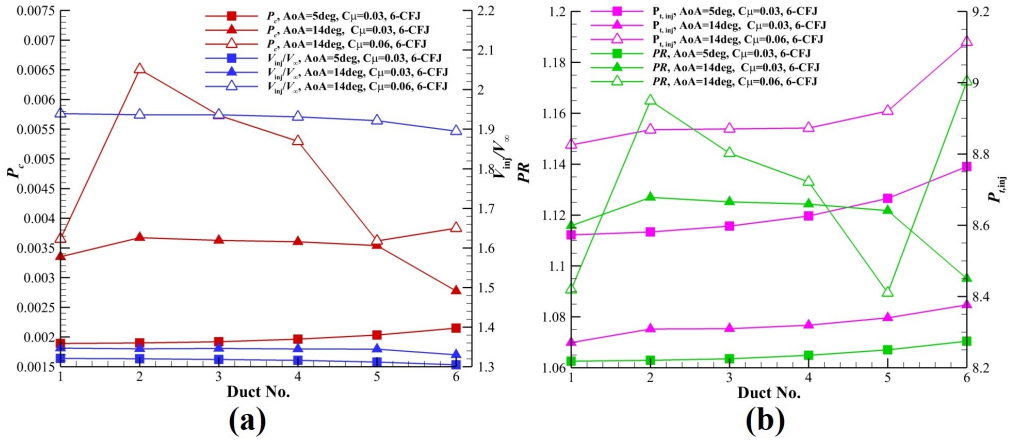

Figure 7: Power coefficient, injection velocity, CFJ duct pressure ratio and injection slot total pressure versus CFJ set number of 6-CFJ wing at varied flow conditions.

To compare the spanwise variation of flow characteristics in different wings, define four cutaway planes A, B, C and D located at 6.43%s(middle of the next-to-root CFJ Duct), 45%s(middle of the open-slot CFJ space), 83.57%s(middle of the next-to-tip CFJ Duct) and 95%s(middle of the tip solid space) respectively to represent "near-root", "half-s", "near-tip-CFJ" and "near-tip-solid" locations, as shown in Fig. 8.

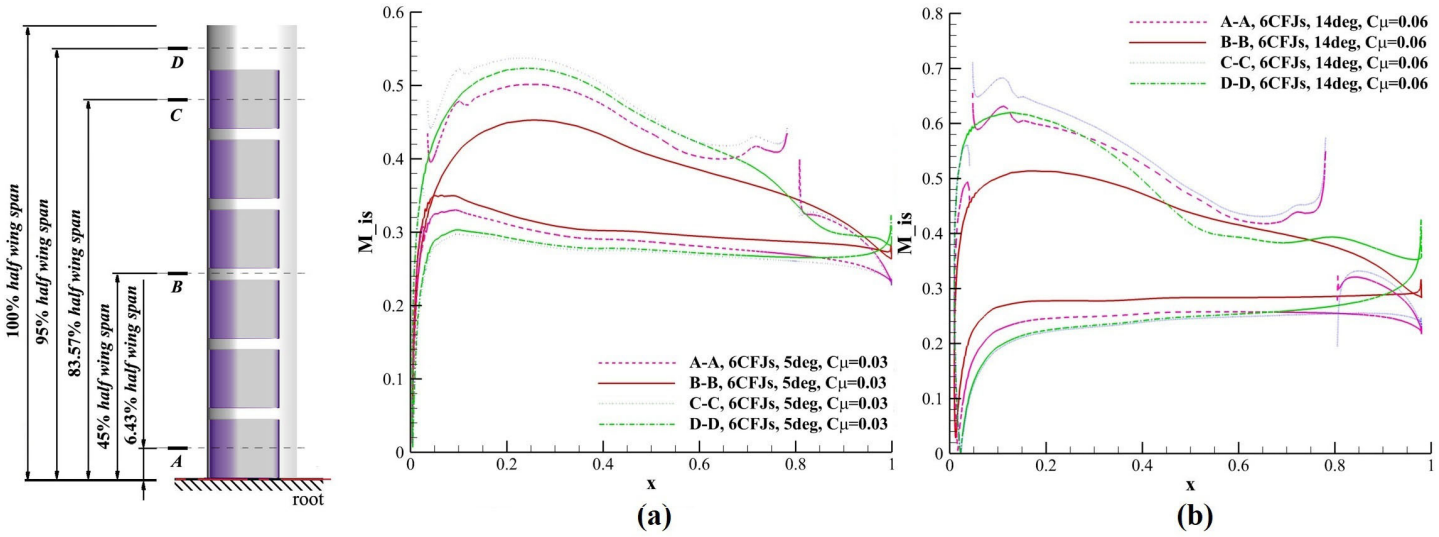

Figure 8: Isentropical Mach number distribution at four cutaway planes under the condition of AoA=5°, C_μ=0.03(a) and AoA=14°, C_μ=0.06(b).

The isentropical Mach number around wing profile at four cutaway planes are plotted as shown in Fig. 8, which denotes the pressure distribution around the profiles. It can be seen that, no matter what flow condition is, the largest pressure difference is always found in tip solid region, while the smallest pressure difference is found in half-s solid region. From Fig. 9, 10, 11 and 12 it can be also seen that, a "solid gap" section except tip that was not covered by co-flow jet will always introduce local separation at high AoAs, even it's as narrow as 0.129c wide in 6-CFJ case. For discrete CFJ wings with less CFJ sets and wider solid gap, such separation is even worse.

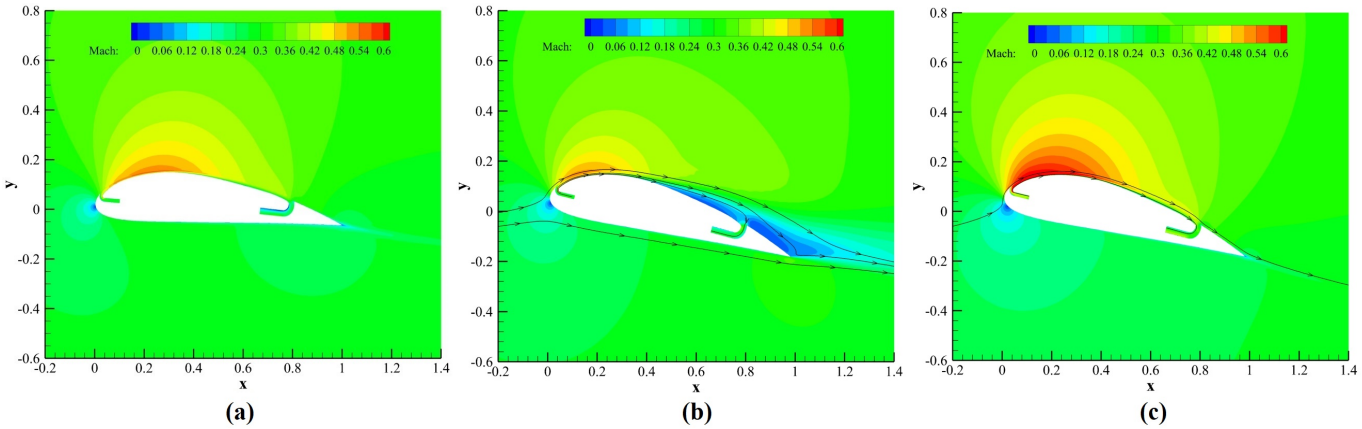

Figure 9: Mach number contours around 6-CFJ-NACA-6421 at cutaway plane A under the condition of AoA=5°, C_μ=0.03(a), AoA=14°, C_μ=0.03(b) and AoA=14°, C_μ=0.06(c).

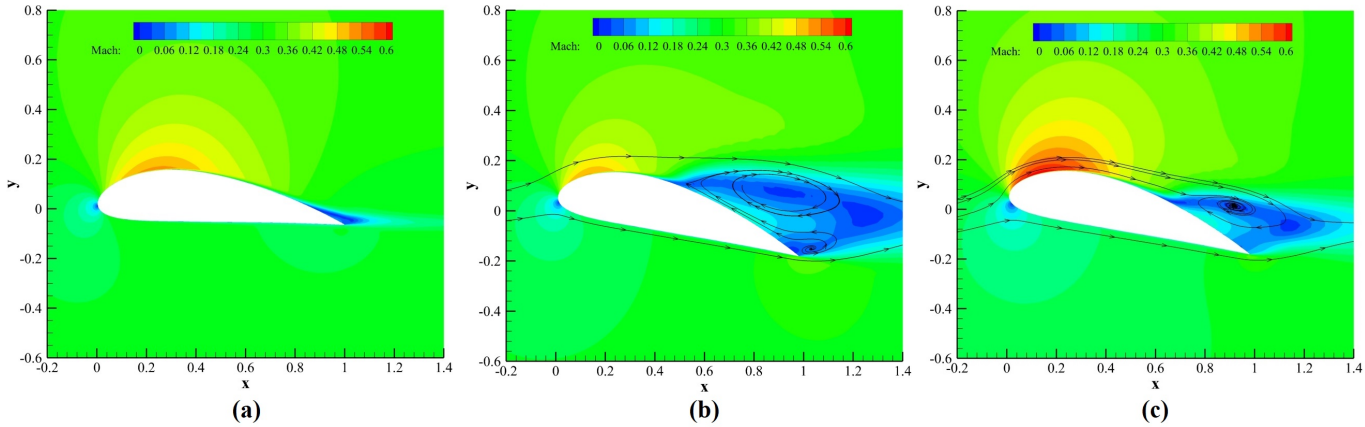

Figure 10: Mach number contours around 6-CFJ-NACA-6421 at cutaway plane B under the condition of AoA=5°, C_μ=0.03(a), AoA=14°, C_μ=0.03(b) and AoA=14°, C_μ=0.06(c).

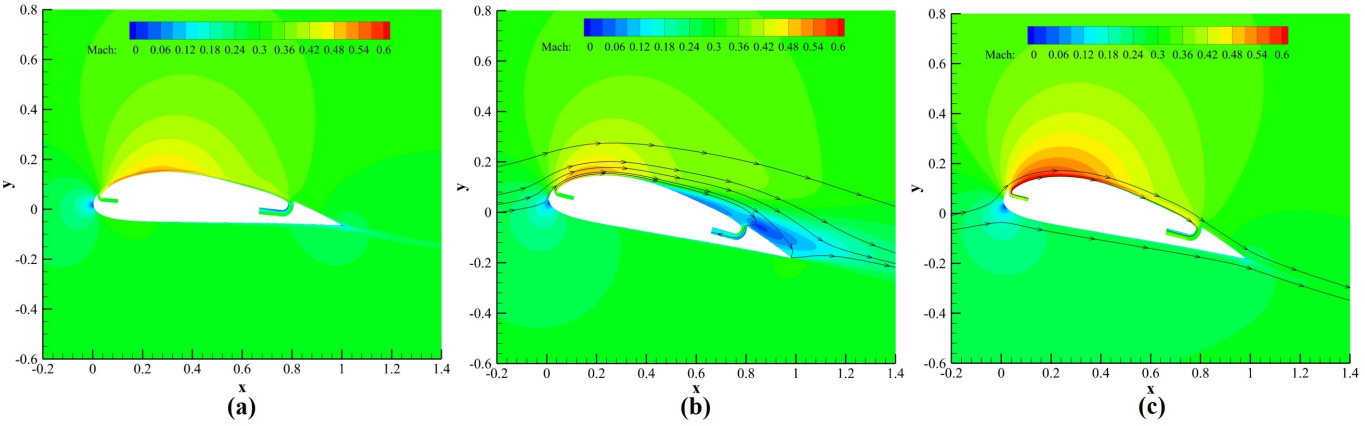

Figure 11: Mach number contours around 6-CFJ-NACA-6421 at cutaway plane C under the condition of AoA=5°, C_μ=0.03(a), AoA=14°, C_μ=0.03(b) and AoA=14°, C_μ=0.06(c).

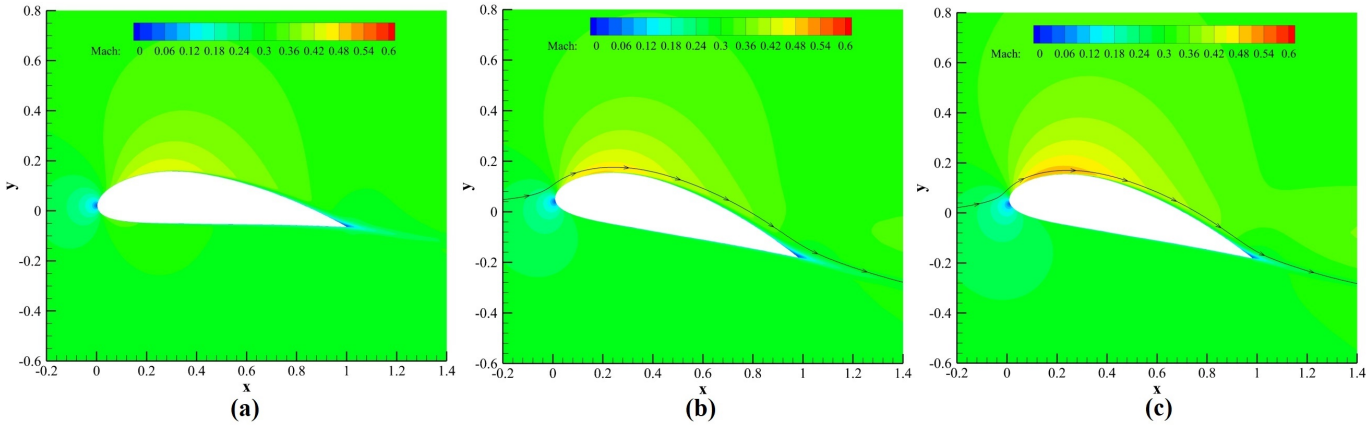

Figure 12: Mach number contours around 6-CFJ-NACA-6421 at cutaway plane D under the condition of AoA=5°, C_μ=0.03(a), AoA=14°, C_μ=0.03(b) and AoA=14°, C_μ=0.06(c).

4.5 Trend of Performance Variation as CFJ Set Decreases

Lift and power coefficients of all four discrete CFJ wings and open-slot CFJ(treated as "7-CFJ") under three flow conditions are plotted in Fig. 13.

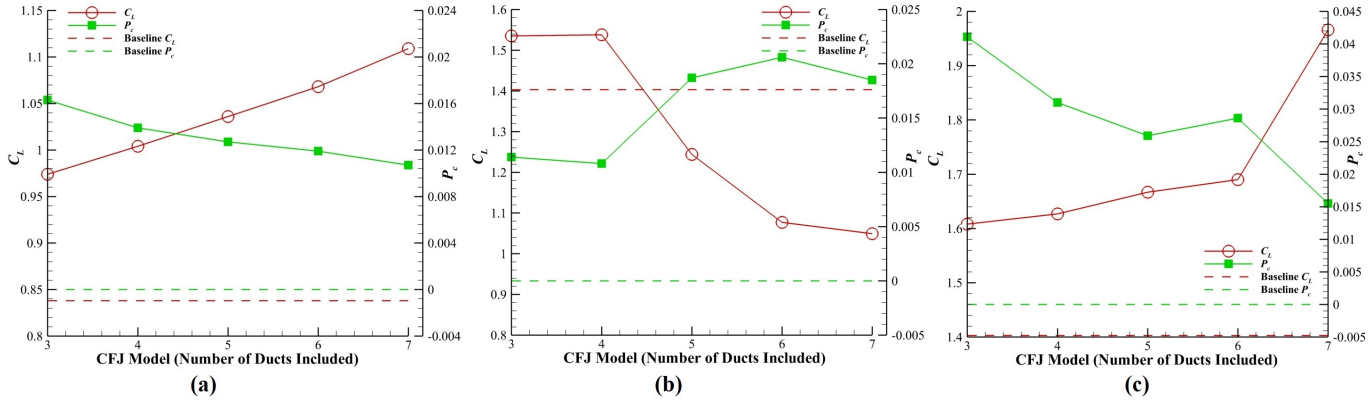

Figure 13: Lift and power coefficients of 3-, 4-, 5-, 6-CFJ, open-slot CFJ ("7-CFJ") compared with baseline NACA-6421 wing at AoA=5° and C_μ=0.03(a), AoA=14° and C_μ=0.03(b), and AoA=14° and C_μ=0.06(c).

It can be noticed that, under the condition of AoA=5° and C_μ=0.03, C_L drops almost linearly as CFJ-coverage factor R decreases, while P_c gradually and almost linearly increases in a narrow range. For 3-CFJ case, with R = 0.386 or 61.4% of suction surface area including tip uncovered by Co-flow jet, The CFJ lift enhancement effect receives a penalty of only 49.8%. For 4-CFJ case, with 42.9% of suction surface area including tip uncovered by Co-flow jet, The CFJ lift enhancement effect receives a penalty of 38.7%.

Fig. 14 explains the considerable difference between C_L of 3-CFJ and 6-CFJ, where blue regions near trailing edges are iso-surfaces of M=0.02, which show a low speed zone caused by minor separation exists around whole TE where there is no CFJ duct upstream, except tip region. Fig. 14 further illustrates that, no matter the solid parts of suction surface is wide(a) or narrow(b), there are always minimum separation and small vortices existing near the trailing edge of them, which explains the slight reduce of lift enhancement effect. It can be expected that,

by removing the solid gap dividing jet flows and introducing a united suction surface transportation and suction slot throughout the span, the flow characteristics in these regions can be improved.

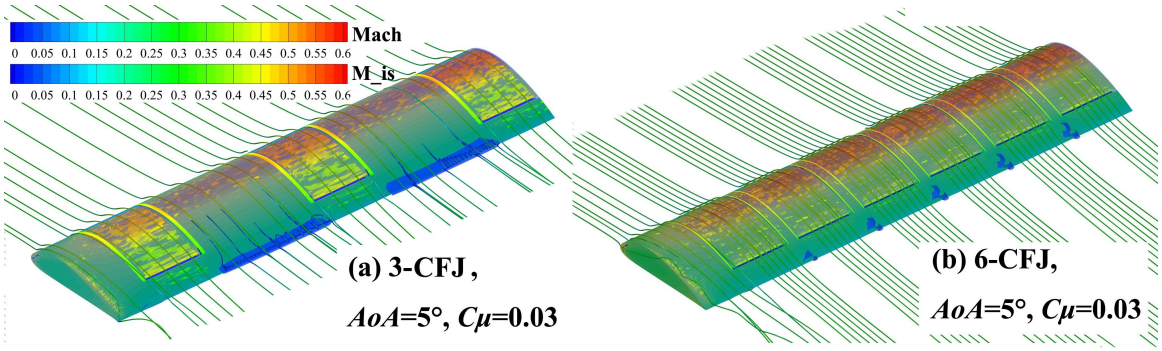

Figure 14: Comparison of the flowfield around 3-CFJ(a) and 6-CFJ(b) at AoA=5° and C_μ=0.03. Streamlines contoured by Mach number, wing surfaces contoured by isentropical Mach number, and a layer of iso-surface M=0.02 is displayed to show the dead-water zone near TEs.

At AoA=14° and C_μ = 0.06, C_L drops dramatically with even only one of seven CFJ sets removed, and P_C significantly increases as R increases. Moreover it can be noticed that, at AoA=14° and C_μ=0.03, which is not enough to eliminate separation in CFJ-covered regions, 3- and 4-CFJ configuration turns out to be still able to improve lift for 9.6% and maintain lower P_c, while open-slot CFJ and discrete CFJs with larger Rs generate negative lift enhancement effect. Fig 15 shows the flowfield around those three geometroes. It can be inferred that, there is a threshold of $C_{\mu,duct}$ to create a separation-eliminated region at downstream and thus generate lift enhancement, which is no smaller than 0.02. This result seems partly verified Dano's conclusion that DCFJ with 1/2 injection blockage can increase lift than open-slot CFJ[30]. Meanwhile, in spanwise direction, CFJ flow control failures always start near root.

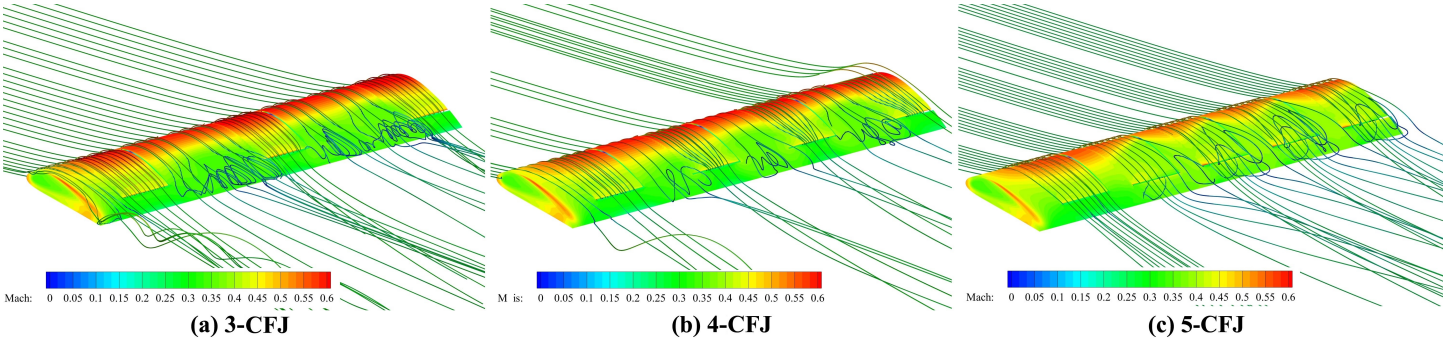

Figure 15: Comparison of the flowfield around 3-, 4- and 5-CFJ at AoA=14°, C_μ=0.03. Streamlines contoured by M, wall surfaces contoured by isentropical Mach number.

C_L/C_D and $(C_L/C_D)_c$ of the mentioned four discrete CFJ wings and open-slot CFJ(treated as "7-CFJ") under three flow conditions are plotted in Fig. 16. Similar as the lift coefficient case, at low AoA, C_L/C_D and $(C_L/C_D)_c$ drops gradually and almost linearly as CFJ-coverage factor R decreases, while at large AoA with large C_μ situation, $(C_L/C_D)_c$ drops significantly with even only one CFJ set removed, and except for the open-slot CFJ configuration, 3-CFJ turns out to be the best one when judged by C_L/C_D, while 5-CFJ has the highest $(C_L/C_D)_c$. Under the stall condition, discrete CFJ with large Rs tends to undermine C_L/C_D and $(C_L/C_D)_c$ performance, while 3-CFJ shows the best result for both.

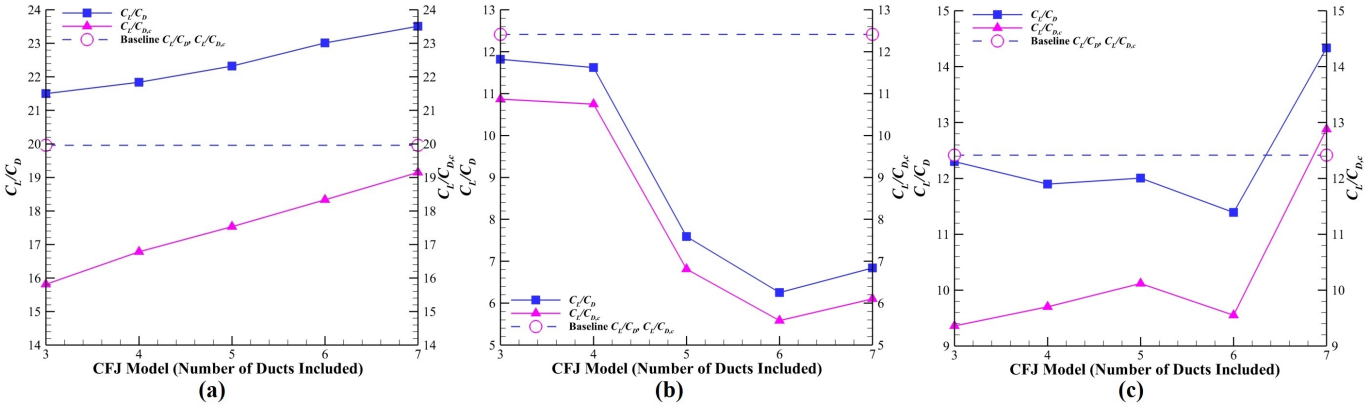

Figure 16: C_L/C_D and $(C_L/C_D)_c$ of 3-, 4-, 5-, 6-CFJ, open-slot CFJ ("7-CFJ") compared with baseline NACA-6421 wing at AoA=5° and C_μ=0.03(a), AoA=14° and C_μ=0.03(b), and AoA=14° and C_μ=0.06(c).

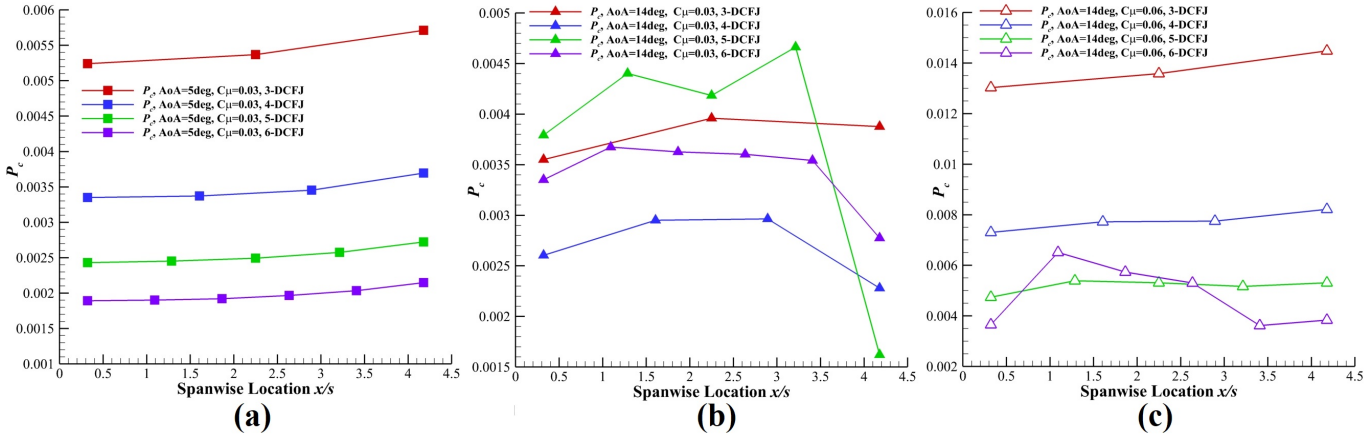

Figure 17: Breakdown of P_c contribution in each duct of 3-, 4-, 5- and 6-CFJ wings.

A breakdown comparison of P_c contribution in each duct of 3-, 4-, 5- and 6-CFJ is plotted in Fig. 17. The x-axis shows the centerpoint coordinate of the different configurations' ducts in spanwise locations on the same baseline wing geometry. It can be clearly seen that, with identical C_μ given to each slot, the CFJ set closest to tip consumes most pump power if the flow is attached over all ducts, while it's opposite for the CFJ sets near the root. It can be inferred that, the lift and power consumption performance of the whole discrete CFJ wing can be optimized by rearranging the C_μ on each discrete CFJ sets properly.

5 Conclusions

The spanwise distribution of Co-Flow Jet (CFJ) for a straight wing at freestream Mach number of 0.30, C_μ=0.03 and 0.06 at angles of attack (AOA) of 5° and 14° is numerically studied. Five configurations with different CFJ distributions along the wing span are investigated. Among these configurations, CFJ-covered suction surface area varies from 38.5% to 90% of the wing span in continuous or discrete distribution along the span.

There are two aspects of conclusions can be made from the study. On the one hand, due to the existence of

vortex near the tip, CFJ in this region does not provide as large lift enhancement as in near-root places in the span, and an area including as large as 20% of wing span can thus be freed from CFJ device to satisfy requirements from weight or structural considerations. Also with the help of tip vortices, under normal working condition at a small angle of attack of 5°, a benefit of lift can be acquired with less area covered by CFJ. This is an important conclusion which establishes relationship between lift distribution and CFJ distribution, and will be used in the future CFJ optimization study.

On the other hand, with constant C_μ, the performance of wings mounted with discrete CFJ is penalized with the increasing size of gaps between the discrete jets. Narrow gaps between injection and suction slots of parallel CFJ sets only lead to minor penalty at small AoAs. Still, to optimize the lift performance at large AoAs, these gaps are expected to be minimized or eliminated. Generally, when the CFJ is discretized, the larger angle of attack has more performance penalty. However, at a stall condition with not enough C_μ to eliminate the separation, which is abnormal, a "concentrated" C_μ distribution method can maintain some lift enhancement. This provides a mechanism of saving a CFJ aircraft from a potential stall emergency.

6 Acknowledgment

The simulations are conducted on Pegasus super-computing system at the Center for Computational Sciences (CCS) at the University of Miami.

Disclosure: The University of Miami and Dr. Gecheng Zha may receive royalties for future commercialization of the intellectual property used in this study. The University of Miami is also equity owner in CoFlow Jet, LLC, licensee of the intellectual property used in this study.

References

[1] G.-C. Zha and D. C. Paxton, "A Novel Flow Control Method for Airfoil Performance Enhancement Using Co-Flow Jet." *Applications of Circulation Control Technologies*, Chapter 10, p. 293-314, Vol. 214, Progress in Astronautics and Aeronautics, AIAA Book Series, Editors: Joslin, R. D. and Jones, G.S., 2006.

[2] G.-C. Zha, W. Gao, and C. Paxton, "Jet Effects on Co-Flow Jet Airfoil Performance," *AIAA Journal, No. 6,*, vol. 45, pp. 1222–1231, 2007.

[3] G.-C. Zha, C. Paxton, A. Conley, A. Wells, and B. Carroll, "Effect of Injection Slot Size on High Performance Co-Flow Jet Airfoil," *AIAA Journal of Aircraft*, vol. 43, 2006.

[4] G.-C. Zha, B. Carroll, C. Paxton, A. Conley, and A. Wells, "High Performance Airfoil with Co-Flow Jet Flow Control," *AIAA Journal*, vol. 45, 2007.

[5] Wang, B.-Y. and Haddoukessouni, B. and Levy, J. and Zha, G.-C., "Numerical Investigations of Injection Slot Size Effect on the Performance of Co-Flow Jet Airfoil," *Journal of Aircraft*, vol. Vol. 45, No. 6,, pp. pp.2084–2091, 2008.

[6] B. P. E. Dano, D. Kirk, and G.-C. Zha, "Experimental Investigation of Jet Mixing Mechanism of Co- Flow Jet Airfoil." AIAA-2010-4421, 5th AIAA Flow Control Conference, Chicago, IL, 28 Jun - 1 Jul 2010.

[7] B. P. E. Dano, G.-C. Zha, and M. Castillo, "Experimental Study of Co-Flow Jet Airfoil Performance Enhancement Using Micro Discreet Jets." AIAA Paper 2011-0941, 49th AIAA Aerospace Sciences Meeting, Orlando, FL, 4-7 January 2011.

[8] A. Lefebvre, B. Dano, W. Bartow, M. Fronzo, and G. Zha, "Performance and energy expenditure of coflow jet airfoil with variation of mach number," *Journal of Aircraft*, vol. 53, no. 6, pp. 1757–1767, 2016.

[9] A. Lefebvre, G-C. Zha, "Numerical Simulation of Pitching Airfoil Performance Enhancement Using Co-Flow Jet Flow Control," *AIAA paper 2013-2517*, June 2013.

[10] A. Lefebvre, G-C. Zha, "Cow-Flow Jet Airfoil Trade Study Part I : Energy Consumption and Aerodynamic Performance," *32nd AIAA Applied Aerodynamics Conference, AIAA AVIATION Forum, AIAA 2014-2682*, June 2014.

[11] A. Lefebvre, G-C. Zha, "Cow-Flow Jet Airfoil Trade Study Part II : Moment and Drag," *32nd AIAA Applied Aerodynamics Conference, AIAA AVIATION Forum, AIAA 2014-2683*, June 2014.

[12] Lefebvre, A. and Zha, G.-C., "Trade Study of 3D Co-Flow Jet Wing for Cruise Performance." AIAA Paper 2016-0570, AIAA SCITECH2016, AIAA Aerospace Science Meeting, San Diego, CA, 4-8 January 2016.

[13] Zha, G.C., Shen, Y.Q. and Wang, B.Y., "An improved low diffusion E-CUSP upwind scheme ," *Journal of Computer and Fluids*, vol. 48, pp. 214–220, Sep. 2011.

[14] Shen, Y.Q., and Zha, G.C., "Large Eddy Simulation Using a New Set of Sixth Order Schemes for Compressible Viscous Terms," *Journal of Computational Physics*, vol. 229, pp. 8296–8312, doi:10.1016/j.jcp.2010.07.017, 2010.

[15] Shen, Y.-Q. and Zha, G.-C. and Chen, X.-Y., " High Order Conservative Differencing for Viscous Terms and the Application to Vortex-Induced Vibration Flows," *Journal of Computational Physics*, vol. 228(2), pp. 8283–8300, 2009.

[16] Shen, Y.-Q. and Zha, G.-C. , " Improvement of the WENO Scheme Smoothness Estimator," *International Journal for Numerical Methods in Fluids*, vol. DOI:10.1002/fld.2186, 2009.

[17] Y.-Q. Shen, G.-C. Zha, and B.-Y. Wang, "Improvement of Stability and Accuracy of Implicit WENO Scheme ," *AIAA Journal*, vol. 47, pp. 331–344, 2009.

[18] G.-C. Zha, Y. Shen, and B. Wang, "An improved low diffusion e-cusp upwind scheme," *Computers & fluids*, vol. 48, no. 1, pp. 214–220, 2011.

[19] G.-C. Zha and E. Bilgen, "Numerical Solutions of Euler Equations by Using a New Flux Vector Splitting Scheme ," *International Journal for Numerical Methods in Fluids*, vol. 17, pp. 115–144, 1993.

[20] X.-Y. Chen and G.-C. Zha, "Fully Coupled Fluid-Structural Interactions Using an Efficient High Solution Upwind Scheme." AIAA Paper 2004-2331, to appear in Journal of Fluids and Structures, 2005.

[21] B.-Y. Wang and G.-C. Zha, "A General Sub-Domain Boundary Mapping Procedure For Structured Grid CFD Parallel Computation," *AIAA Journal of Aerospace Computing, Information, and Communication*, vol. 5, No.11, pp. 2084–2091, 2008.

[22] Lefebvre, A. and Dano, B. and Bartow, W. and Di Franzo, M. and Zha, G.-C., "Performance Enhancement and Energy Expenditure of Co-Flow Jet Airfoil with Variation of Mach Number." AIAA Paper 2013-0490, AIAA Journal of Aircraft, DOI: 10.2514/1.C033113, 2016.

[23] Y. Yang and G. Zha, "Super-lift coefficient of active flow control airfoil: What is the limit?," p. 1693, 2017.

[24] G. Z. Kewei Xu, "High control authority 3d aircraft control surfaces using co-flow jet," *AIAA Journal of Aircraft*, vol. DOI 10.1007/s12650-010-0057-7, 2020.

[25] G. Zha, W. Gao, and C.D. Paxton, "Jet Effects on Co-Flow Jet Airfoil Performance," *AIAA Journal*, vol. 45, pp. 1222–1231, 2007.

[26] Liu, Z.-X. and Zha, G.-C., "Transonic Airfoil Performance Enhancement Using Co-Flow Jet Active Flow Control." AIAA Paper 2016-3066, AIAA Aviation, June 13-17 2016.

[27] Lefebvre, A. and Zha, G.-C. , "Design of High Wing Loading Compact Electric Airplane Utilizing Co-Flow Jet Flow Control." AIAA Paper 2015-0772, AIAA SciTech2015: 53nd Aerospace Sciences Meeting, Kissimmee, FL, 5-9 Jan 2015.

[28] Yang, Yunchao and Zha, Gecheng, "Super-Lift Coefficient of Active Flow Control Airfoil: What is the Limit?," *AIAA Paper 2017-1693, AIAA SCITECH2017, 55th AIAA Aerospace Science Meeting, Grapevine, Texas*, p. 1693, 9-13 January 2017.

[29] Y. Wang and G. Zha, "Study of mach number effect for 3d co-flow jet wings at cruise conditions," in *AIAA Scitech 2020 Forum*, p. 0045, 2020.

[30] B. Dano, A. Lefebvre, and G. Zha, "Mixing mechanism of a discrete co-flow jet airfoil," p. 3097, 2011.